TECHNICAL MEMORANDUM

X-437

FREE-FLIGHT TESTS TO A MACH NUMBER OF 1.5 OF SLENDER

TRIANGULAR PYRAMID REENTRY CONFIGURATIONS

By Joseph H. Judd and Gerard E. Woodbury

Langley Research Center
Langley Field, Va.

NATIONAL AERONAUTICS AND SPACE ADMINISTRATION

WASHINGTON   March 1961

CONFIDENTIAL

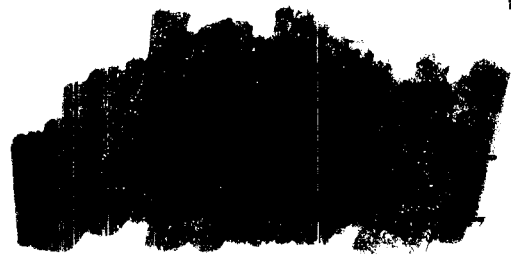NATIONAL AERONAUTICS AND SPACE ADMINISTRATION

TECHNICAL MEMORANDUM X-437

FREE-FLIGHT TESTS TO A MACH NUMBER OF 1.5 OF SLENDER

TRIANGULAR PYRAMID REENTRY CONFIGURATIONS*

By Joseph H. Judd and Gerard E. Woodbury

SUMMARY

14766

Rocket-propelled triangular configurations have been flown to a Mach number of 1.5 and to Reynolds numbers, based on wing mean aerodynamic chord (two-thirds body length), of 59×10^6. Four small models were flown to a Mach number of 1.2 by the helium-gun technique.

Measured lift and pitching-moment-coefficient slopes for small angles were approximately the same as predicted by linearized theory at an average Mach number of 1.45. The models were dynamically stable for small angular disturbances where the rolling velocity was near zero.

INTRODUCTION

The basic approach to atmospheric reentry flight has been to use high drag coefficients to dissipate energy to the atmosphere. When the reentry vehicle has reached velocities where aerodynamic heating presents a soluble problem, the transition of the vehicle from a high-drag configuration to an efficient lifting vehicle becomes desirable. Various configurations have been proposed for hypersonic flight and lifting reentry trajectories and range from simple geometric shapes such as the cone to wing-body-tail configurations. The Langley Research Center is conducting programs to investigate the aerodynamic characteristics of these proposed configurations. (For example, see refs. 1 and 2.) As part of these programs, the Langley Research Center is conducting free-flight rocket tests to measure aerodynamic coefficients during oscillating flight. The present report presents the flight-test data for a slender right-triangular pyramid model which was tested.

---

*Title, Unclassified.

CONFIDENTIAL

The test configuration is a simple geometric body having a triangular planform and a cross section which is an equilateral triangle. This configuration represents a triangular wing of wedge airfoil section having an aspect ratio of 0.348. Free-flight tests were made of two rocket-propelled models which were disturbed in flight by pulse rockets in order that the static and dynamic stability at small angles of attack might be determined. Free-flight tests were also made of four helium-gun models.

Flight tests were made at the NASA Wallops Station. The Mach number varied from 0.6 to 1.5 and the Reynolds number, based on mean aerodynamic chord (two-thirds body length), varied from 24×10^6 to 59×10^6 for the rocket models.

SYMBOLS

a_n normal acceleration in g units

a_y transverse acceleration in g units

α angle of attack, deg

β angle of sideslip, deg

C_D total drag coefficient based on equivalent wing area S

$C_{D,0}$ total zero-lift drag coefficient, based on S

$C_{m,t}$ total pitching-moment coefficient about center of gravity, $I_Y\ddot{\theta}/qS\bar{c}$

C_{m_α} pitching-moment-coefficient slope

C_L lift coefficient, based on S

C_{L_α} lift-coefficient slope

C_N normal-force coefficient, $\dfrac{W}{g} a_n/qS$

C_Y side-force coefficient, $\dfrac{W}{g} a_y/qS$

$\bar{c}$	mean aerodynamic chord, ft
M	Mach number
$\ddot{\theta}$	angular acceleration in pitch, radians/sec^2
ρ	air density, slugs/cu ft
$\dot{\phi}$	rolling velocity, radians/sec
q	dynamic pressure, lb/sq ft
R	Reynolds number, based on $\bar{c}$
S	planform area, sq ft
t	time, sec
V	model free-stream velocity, ft/sec
W	weight of the model, lb
X,Y,Z	coordinate axes
$\ddot{\psi}$	angular acceleration in yaw, radians/sec^2
I_X	mass moment of inertia about X-axis, slug-ft^2
I_Y	mass moment of inertia about Y-axis, slug-ft^2
I_Z	mass moment of inertia about Z-axis, slug-ft^2
x_{cg}	location of model center of gravity from reference station 0, ft
$x_{\bar{c}}$	location of leading edge of mean aerodynamic chord from reference station 0, ft
g	acceleration due to gravity, ft/sec^2

MODELS AND APPARATUS

The test configurations were bodies that had a triangular planform and an equilateral triangle cross section. Figures 1 and 2 show drawings and photographs of the rocket test models. Two geometrically

CONFIDENTIAL

similar rocket-propelled models were flown and are designated as models 1 and 2. The geometric characteristics of the model are given in table I; the physical characteristics for models 1 and 2 are given in table II. The base of the rocket model was normal to the center line. The rocket models were made of spruce and foamed plastic covered with fiber glass and plastic. The centers of gravity of the rockets were located on the model center line and the principal axes were the body axes. A single pulse rocket whose nozzle center line was located in the pitch plane on the bottom of the model was used to disturb the models in flight. A single T-55 rocket motor was used to propel the models to supersonic speeds.

Each rocket model had eight instruments which measured angle of attack, angle of sideslip, longitudinal acceleration, normal acceleration, lateral acceleration, angular acceleration in pitch, angular acceleration in sideslip, and angular velocity in roll. An NASA eight-channel telemeter transmitted continuous measurements from each instrument. The flight-attitude indicator which measured angle of attack and angle of sideslip was mounted on a sting at the nose. The base of the flight-attitude indicator was at reference station 0. All instruments were located on the model center line but were located ahead of and behind the center of gravity.

Four small models were made of the triangular configuration and are designated as models 1H, 2H, 3H, and 4H. A drawing of these models is given in figure 3 and the geometrical and physical characteristics are given in tables III and IV. The base was normal to the apex of the triangular cross section. The weights and centers of gravity of these models were varied by machining sections of aluminum and steel. These models were tested by the helium-gun technique. The helium-gun test technique and a description of the equipment used are given in reference 3.

Ground instrumentation for these tests consisted of a CW Doppler velocimeter, NASA modified SCR 584 tracking radar, Reeves modified SCR-584 radar, and FPS-16 tracking radar unit. The model flight path was obtained from the radar sets and the variation of model velocity with time from the velocimeter. A balloon carried a rawinsonde aloft to measure atmospheric properties at the time of the flight tests. The rawinsonde telemetered data were received by a Rawin set AN/GMD-1A. In addition, the variation of the wind velocity and direction with altitude was obtained by the Rawin set.

TESTS

Preflight preparation for the flight tests of the rocket models and the helium-gun models included linear measurement, measurement of the

weight, and the center-of-gravity location. In addition, the rocket
models were suspended below a knife edge and swung as a simple pendulum
to measure the period of the oscillation. The mass moment of inertia
was computed by using this period, air damping of the system, however,
being neglected.

The rocket-propelled models were launched from a zero-length
launcher (fig. 2(b)) at the NASA Wallops Station. The T-55 rocket motor
propelled models 1 and 2 to a peak Mach number of approximately 1.5.
Position radar sets and the CW Doppler velocimeter measured the model
trajectory and velocity, respectively. The variations of the test con-
ditions with time for models 1 and 2 are given in figure 4. The vari-
ations of Reynolds number, based on $\bar{c}$, with Mach number for these
models are given in figure 5. The pulse rockets disturbed the models
from trim flight at about 2.5 seconds after launch during decelerating
flight. Data reduced from telemeter information during this oscillating
portion of the flight are given in figure 6.

The helium-gun models were propelled to supersonic speed from a
helium gun at the NASA Wallops Station. Position radar sets measured
model position in space and the CW Doppler velocimeter measured model
velocity. Drag data were obtained from the CW Doppler velocimeter by
the technique described in reference 4. All velocities were corrected
for the wind component obtained from the rawinsonde. The flights of all
the helium-gun models were disturbed upon separation from the cradle and
push plate. Models 3H and 4H had drag coefficients more than twice the
magnitude of models 1H and 2H. Since it is thought that models 3H and 4H
were unstable because of the rearward location of the center of gravity
(table IV), drag data were not presented for these models. The variation
of test Reynolds numbers with Mach number for models 1H and 2H is also
shown in figure 5.

ANALYSIS OF DATA

Drag coefficients for the rocket models 1 and 2 were obtained by
using the CW Doppler velocimeter technique and also by using the longi-
tudinal accelerometer measurements. For the region of relatively slow
drag-coefficient change, both measurements agreed. Where the drag
coefficient changed rapidly as in the transonic region, the drag coef-
ficients obtained from accelerometer measurements were used.

Analysis of the data obtained during oscillating flight followed
the methods described in reference 5. Both the measured angle of
attack α and the angle of sideslip β were transferred to values at
the center of gravity of the rocket models by the method described in

reference 6. Furthermore, the components of linear accelerations caused by model angular accelerations and velocities were subtracted from the measured accelerations. Thus, all the force and moment coefficients presented herein are those for the center of gravity of the models.

The total pitching moment was computed by using the angular acceleration in pitch. A two-degree-of-freedom analysis, as described in references 5 and 7, was attempted in order to separate the dynamic pitch damping from the total pitching-moment coefficient C_{m_α} computed from the flight data. However, since the decay of disturbances was not uniform, these terms have been neglected for the pitching-moment coefficient data presented herein. When the average values of pitch damping were used, the error in pitching-moment-coefficient slope caused by neglect of the damping contribution was smaller than 3 percent.

ACCURACY

In order to establish telemeter instrument accuracies, statistical data have been compiled on flight-instrument measurements over a number of years, and on the basis of the information obtained, the maximum probable error is believed to be 1 percent of the full-scale calibrated range for the telemetered measurements. These maximum probable errors in measurements have been used to compute the errors in the normal force, side force, drag, and total pitching-moment coefficients for the average Mach number 1.4 during a period of oscillating flight. These computed errors are as follows:

Mach number	C_N	C_Y	C_D	$C_{m,t}$	α, deg	β, deg
1.4	±0.009	±0.009	±0.001	±0.0005	±0.5	±0.5

The velocity measured by the CW Doppler velocimeter is known to have an error of less than 1 percent at supersonic speeds and less than 2 percent at subsonic speeds. Since Mach number is determined from velocity, these errors also apply to Mach number.

No directional stability coefficients are presented because the experimental error was large compared with the measured yawing moments obtained during the flight.

RESULTS AND DISCUSSION

The variation of total zero-lift drag coefficient with Mach number for rocket models 1 and 2 is presented in figure 7 and for helium-gun models 1H and 2H in figure 8. Angles of attack and sideslip for models 1H and 2H were not known. For purposes of comparison, the average drag coefficients for models 1 and 2 and for models 1H and 2H are plotted together with experimental drag coefficients from reference 1 in figure 9. The three experimental sets of data for the triangular pyramids exhibit appreciable differences in total drag coefficient, the closest agreement being between the helium-gun models and those of reference 1. The Reynolds number based on $\bar{c}$ for reference 1 was 4.83×10^6 at a Mach number of 1.41 and 4.02×10^6 at a Mach number of 2.01. The helium-gun Reynolds numbers were similar, although they are in the region where large variations in base pressure coefficients occurred for small differences in Reynolds numbers (see ref. 8). Models 1 and 2 had high Reynolds numbers (fig. 5) and according to reference 8 are in a region where the variation of base pressure coefficient with Reynolds number is small. By using reference 8, the friction drag coefficients of the rocket models at Mach numbers of 0.9 and 1.1 were estimated to be 0.0025 lower than those of the helium-gun models. This condition accounted for 50 percent of the measured difference in drag coefficients at $M < 0.9$ and 25 percent at $M > 1.1$.

An estimate of the total drag coefficient was made for the rocket models using base pressure coefficients from reference 9 and skin-friction coefficients from reference 8. The pressure drag was estimated by using linearized theory for half of a wedge airfoil (ref. 10) and also by using the pressure coefficients for the equivalent body of revolution (ref. 11) which was a 3.8° half-angle cone. The cone surface pressures were obtained from reference 12. The total estimated drag coefficients are also plotted in figure 9 and it appears that reasonably accurate drag estimates for these configurations can be made at supersonic speeds.

Figure 6 presents the angular motions, force coefficients, and angular accelerations of models 1 and 2 after they were disturbed in flight by the pulse rockets. From these data, it can be seen that the triangular pyramid was statically and dynamically stable for small disturbances ($\alpha = \pm 2^\circ$) and for near zero rolling velocity.

The variation of lift, drag, and total pitching-moment coefficients with angle of attack obtained during pitching motions are shown in figure 10. Measured values of C_{L_α} from reference 1, the C_{L_α} of model 2, and linearized theory for plane triangular wings from reference 13 are compared in figure 11. Agreement is good between $M = 1.39$ and

M = 1.50. The lift-curve slopes are about 50 percent greater than those of a body of revolution $\left(C_{L_\alpha} = 0.0053 \text{ per degree}\right)$.

The total pitching-moment coefficient given in figure 10 includes contributions due to angular velocities of the configuration. The period of the short-period pitching oscillation was also used to compute the pitching-moment-coefficient slope by the method of reference 7. These C_{m_α} values for models 1 and 2 agreed and had a value of -0.048 per radian at the average Mach number of 1.45. The location of the aerodynamic center was at $0.49\bar{c}$ or very close to predicted values of the two-thirds length of a cone and $0.5\bar{c}$ for a slender triangular wing.

CONCLUDING REMARKS

Free-flight tests of two rocket-propelled triangular pyramids have been made between Mach numbers of 0.6 and 1.5 and for Reynolds numbers, based on mean aerodynamic chord, from 24×10^6 to 59×10^6. In addition, four small models were test flown to a Mach number of 1.2 by the helium-gun technique.

Measured lift and pitching-moment-coefficient slopes were in agreement for small angles of attack and at an average Mach number of 1.45 as predicted by linearized theory. Disturbances produced by the pulse rockets decayed rapidly; this condition indicated that the two triangular pyramid configurations were dynamically stable for small disturbances and near zero rolling velocity.

Langley Research Center,
    National Aeronautics and Space Administration,
        Langley Field, Va., October 10, 1960.

REFERENCES

1. Foster, Gerald V.: Static Stability Characteristics of a Series of Hypersonic Boost-Glide Configurations at Mach Numbers of 1.41 and 2.01. NASA TM X-167, 1959.

2. Paulson, John W.: Low-Speed Static Stability and Control Characteristics of a Model of a Right Triangular Pyramid Reentry Configuration. NASA MEMO 4-11-59L, 1959.

3. Hall, James Rudyard: Comparison of Free-Flight Measurements of the Zero-Lift Drag Rise of Six Airplane Configurations and Their Equivalent Bodies of Revolution at Transonic Speeds. NACA RM L53J21a, 1954.

4. Wallskog, Harvey A., and Hart, Roger G.: Investigation of the Drag of Blunt-Nosed Bodies of Revolution in Free Flight at Mach Numbers From 0.6 to 2.3. NACA RM L53D14a, 1953.

5. Gillis, Clarence L., and Mitchell, Jesse L.: Determination of Longitudinal Stability and Control Characteristics From Free-Flight Model Tests With Results at Transonic Speeds for Three Airplane Configurations. NACA Rep. 1337, 1957.

6. Ikard, Wallace L.: An Air-Flow-Direction Pickup Suitable for Telemetering Use on Pilotless Aircraft. NACA TN 3799, 1956. (Supersedes NACA RM L53K16.)

7. Gillespie, Warren, Jr.: Supersonic Aerodynamic Characteristics of a Low-Drag Aircraft Configuration Having an Arrow Wing of Aspect Ratio 1.86 and a Body of Fineness Ratio 20. NACA RM L57A25, 1957.

8. Van Driest, E. R.: Turbulent Boundary Layer in Compressible Fluids. Jour. Aero. Sci., vol. 18, no. 3, Mar. 1951, pp. 145-160, 216.

9. Kurzweg, H. H.: Interrelationship Between Boundary Layer and Base Pressure. Jour. Aero. Sci., vol. 18, no. 11, Nov. 1951, pp. 743-748.

10. Ferri, Antonio: Elements of Aerodynamics of Supersonic Flows. The Macmillan Co., 1949.

11. Jones, Robert T., and Cohen, Doris: Aerodynamics of Wings at High Speeds. Aerodynamic Components of Aircraft at High Speeds. Vol. VII of High Speed Aerodynamics and Jet Propulsion, sec. A, A. F. Donovan and H. R. Lawrence, eds., Princeton Univ. Press, 1957, pp. 3-243.

CONFIDENTIAL

12. Ames Research Staff: Equations, Tables, and Charts for Compressible
     Flow. NACA Rep. 1135, 1953. (Supersedes NACA TN 1428.)

13. Piland, Robert O.: Summary of the Theoretical Lift, Damping-in-Roll,
     and Center-of-Pressure Characteristics of Various Wing Plan Forms
     at Supersonic Speeds. NACA TN 1977, 1949.

TABLE I.- GEOMETRIC PARAMETERS OF ROCKET MODELS

Wing area, sq ft 6.394
Base area, sq ft 0.961
Model length, ft 8.590
Span, ft 1.490
Mean aerodynamic chord, ft 5.730
Leading edge of mean aerodynamic chord, ft 2.860
Aspect ratio 0.348
Sweepback angle of leading edge, deg 85.1

TABLE II.- PHYSICAL CHARACTERISTICS OF ROCKET MODELS

(a) Take-off conditions

Model	Weight, lb	Center of gravity		Mass moments of inertia, slug-ft^2		
		x_{cg}, ft	$(x_{cg} - x_{\bar{c}})/\bar{c}$	I_X	I_Y	I_Z
1	112.50	5.56	0.471	-----	14.08	14.11
2	113.75	5.58	.475	-----	14.32	14.10

(b) Decelerating flight after rocket motor burnout

Model	Weight, lb	Center of gravity		Mass moments of inertia, slug-ft^2		
		x_{cg}, ft	$(x_{cg} - x_{\bar{c}})/\bar{c}$	I_X	I_Y	I_Z
1	79.88	5.03	0.381	0.220	12.12	12.06
2	80.68	5.07	.388	.220	12.32	12.10

CONFIDENTIAL

TABLE III.- GEOMETRIC PARAMETERS OF HELIUM-GUN MODELS

Wing area, sq ft 0.0617
Base area, sq ft 0.0096
Model length, ft 0.851
Span, ft 0.146
Mean aerodynamic chord, ft 0.567
Leading edge of mean aerodynamic chord, ft 0.284

TABLE IV.- PHYSICAL CHARACTERISTICS OF HELIUM-GUN MODELS

Model	Weight, lb	Center of gravity, $\left(x_{cg} - x_{\bar{c}}\right)/\bar{c}$
1H	0.411	0.324
2H	.375	.421
3H	.828	.460
4H	.777	.497
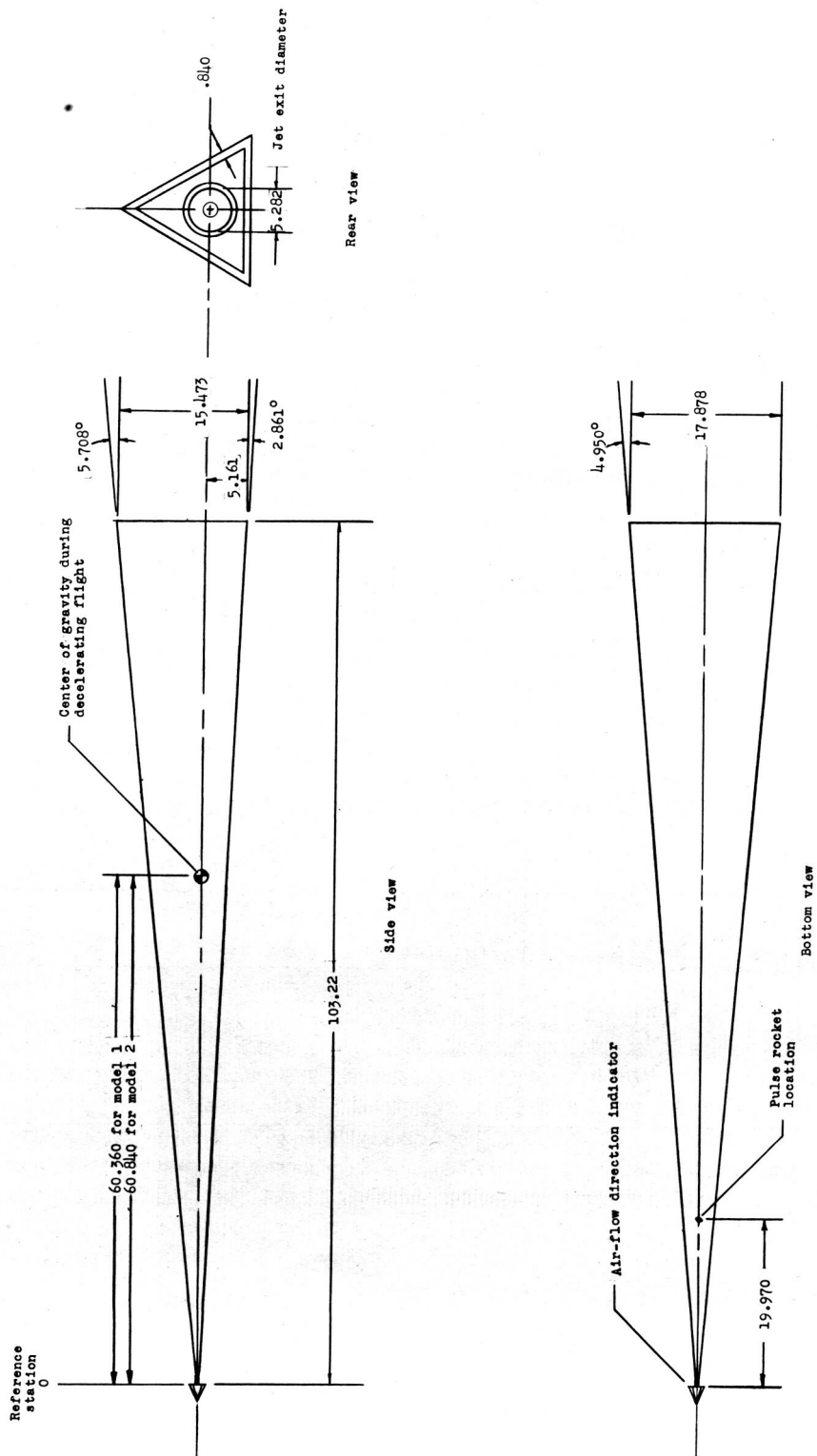
Figure 1.- Three-view drawing of rocket test models. All dimensions are in inches.
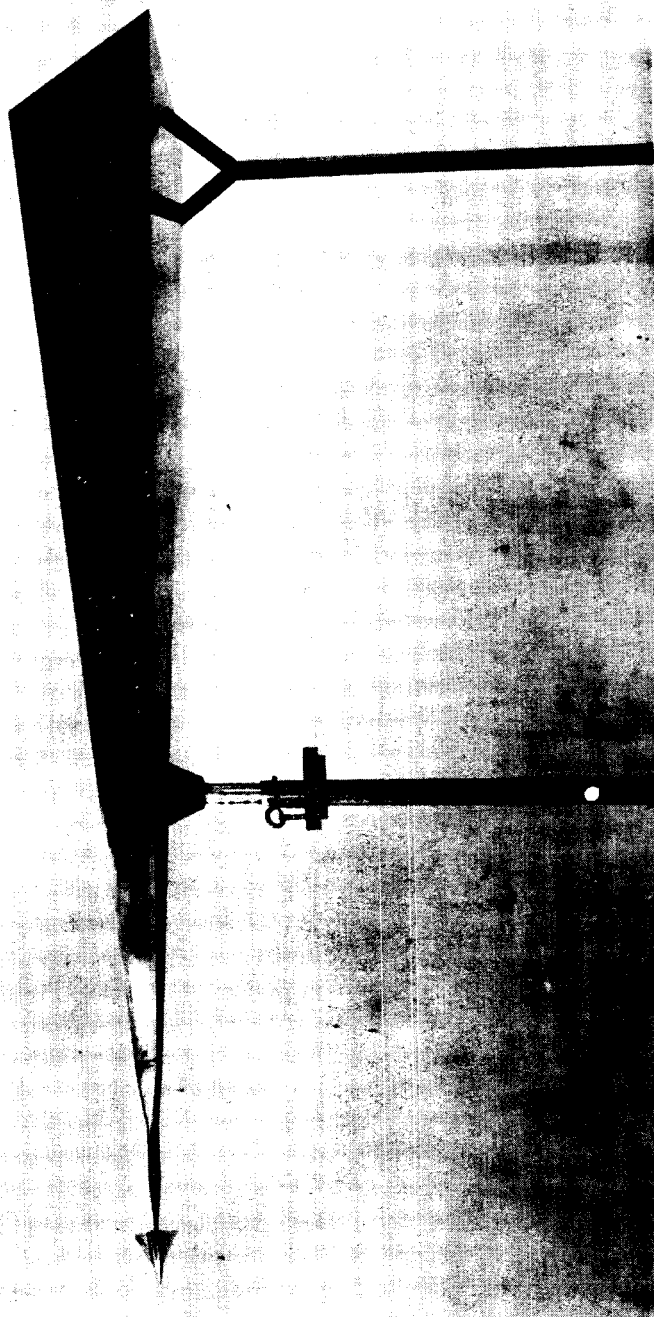
14   CONFIDENTIAL

(a) Front three-quarter side view of model 1.   L-59-2356

Figure 2.- Photographs of rocket test models.

(b) Model 2 on launcher.   L-59-122

Figure 2.- Concluded.
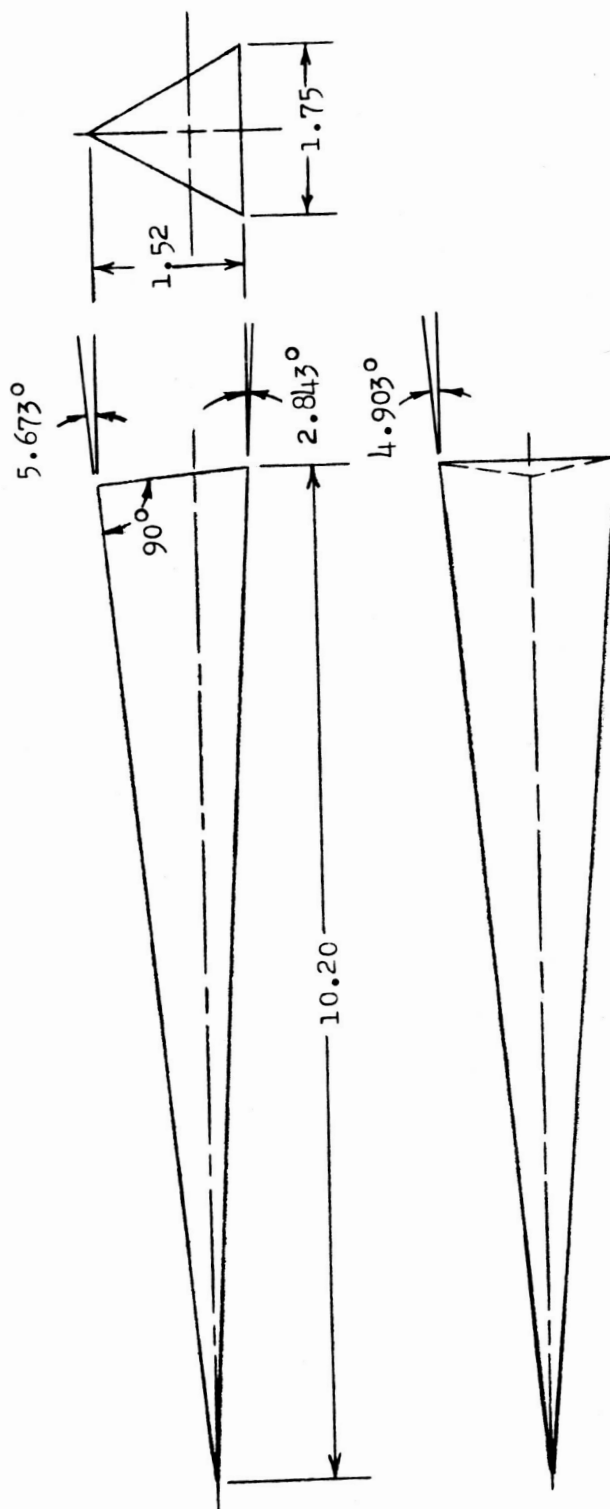
Figure 3.- Three-view drawing of helium-gun models. All dimensions are in inches.
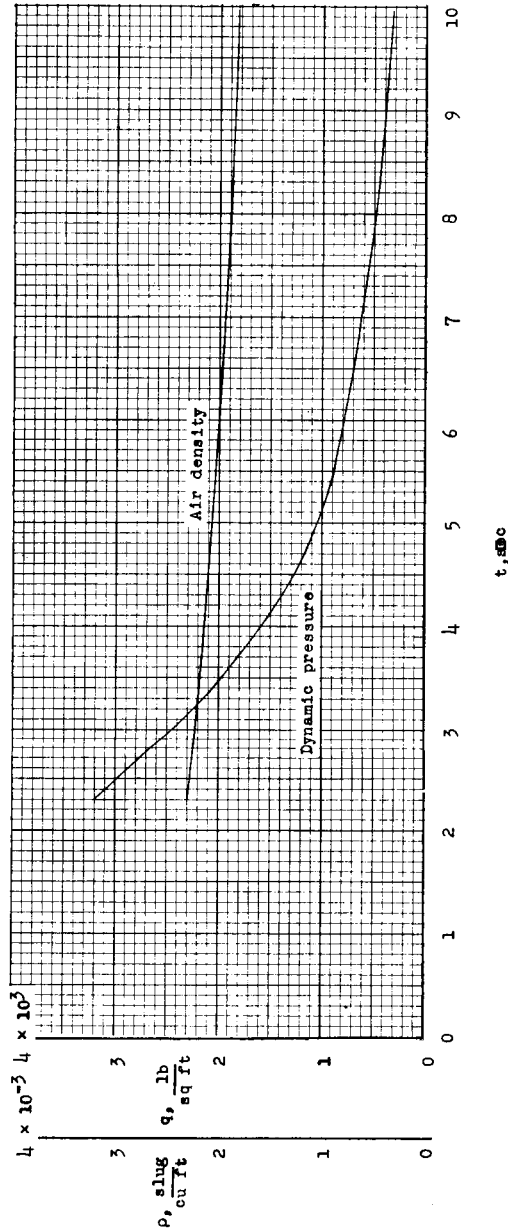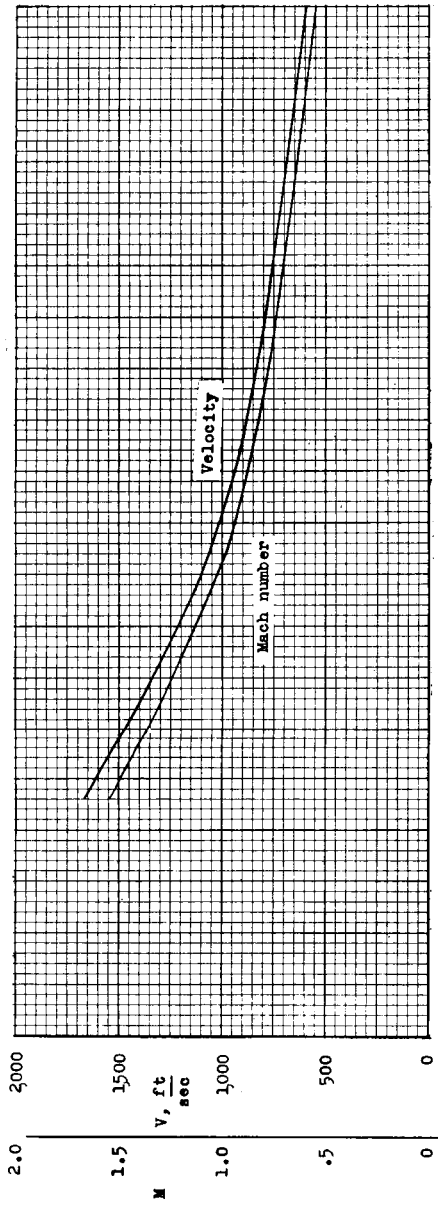
(a) Model 1.

Figure 4.- Variation of Mach number, velocity, dynamic pressure, and air density with time for models 1 and 2.
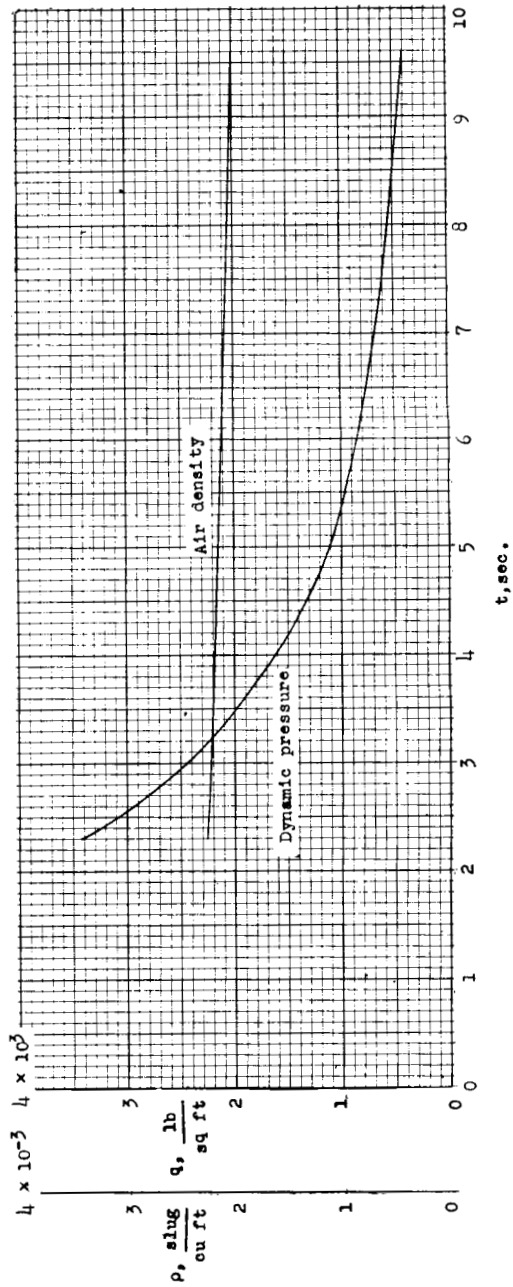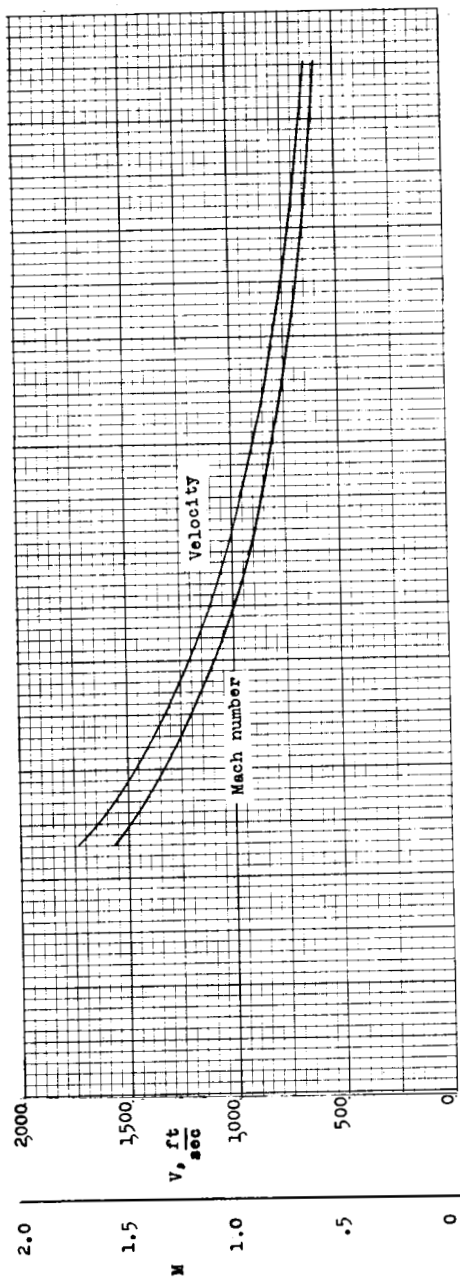
(b) Model 2.

Figure 4.- Concluded.
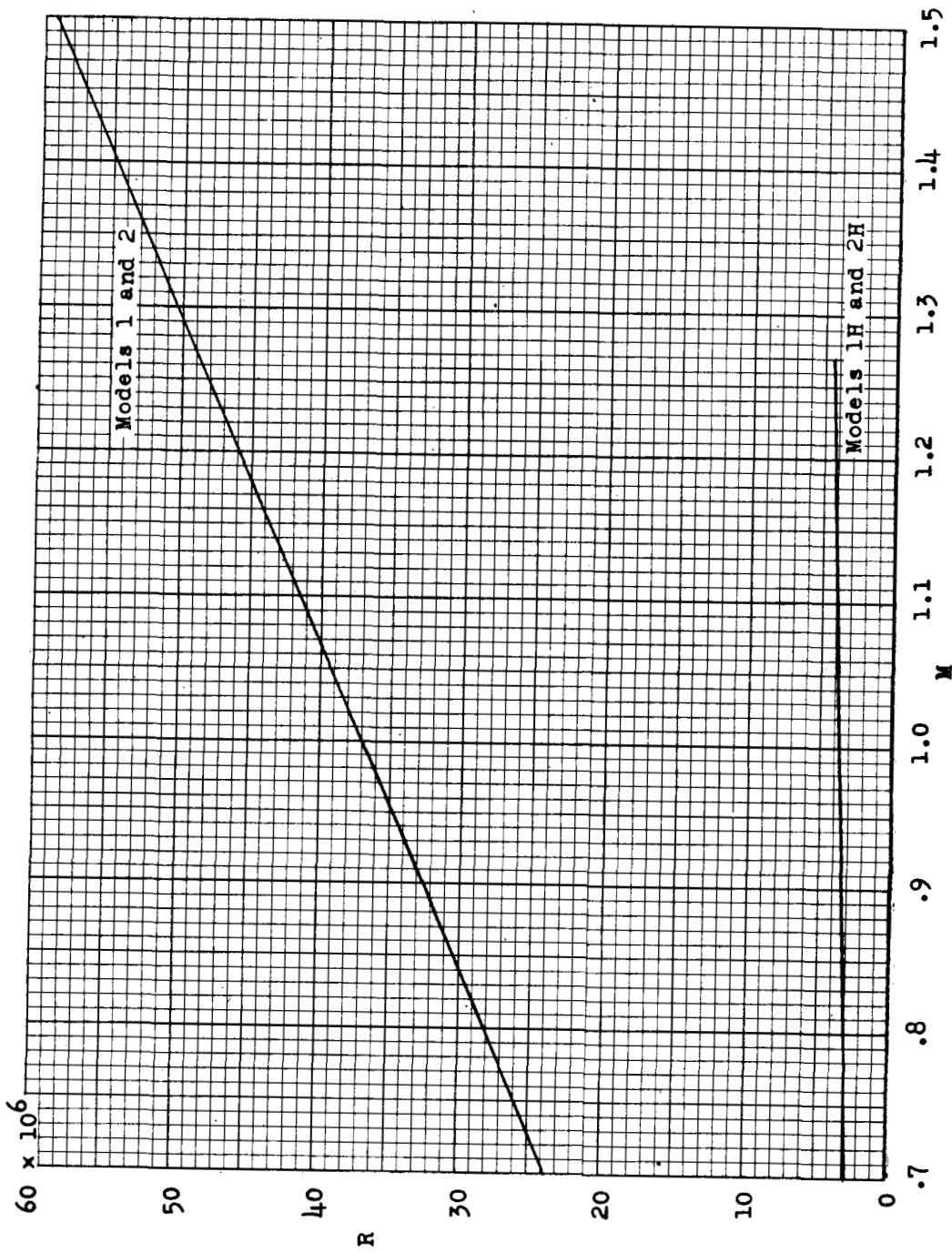
Figure 5.- The variation of Reynolds number, based on mean aerodynamic chord, with Mach number for the flight models.

CONFIDENTIAL
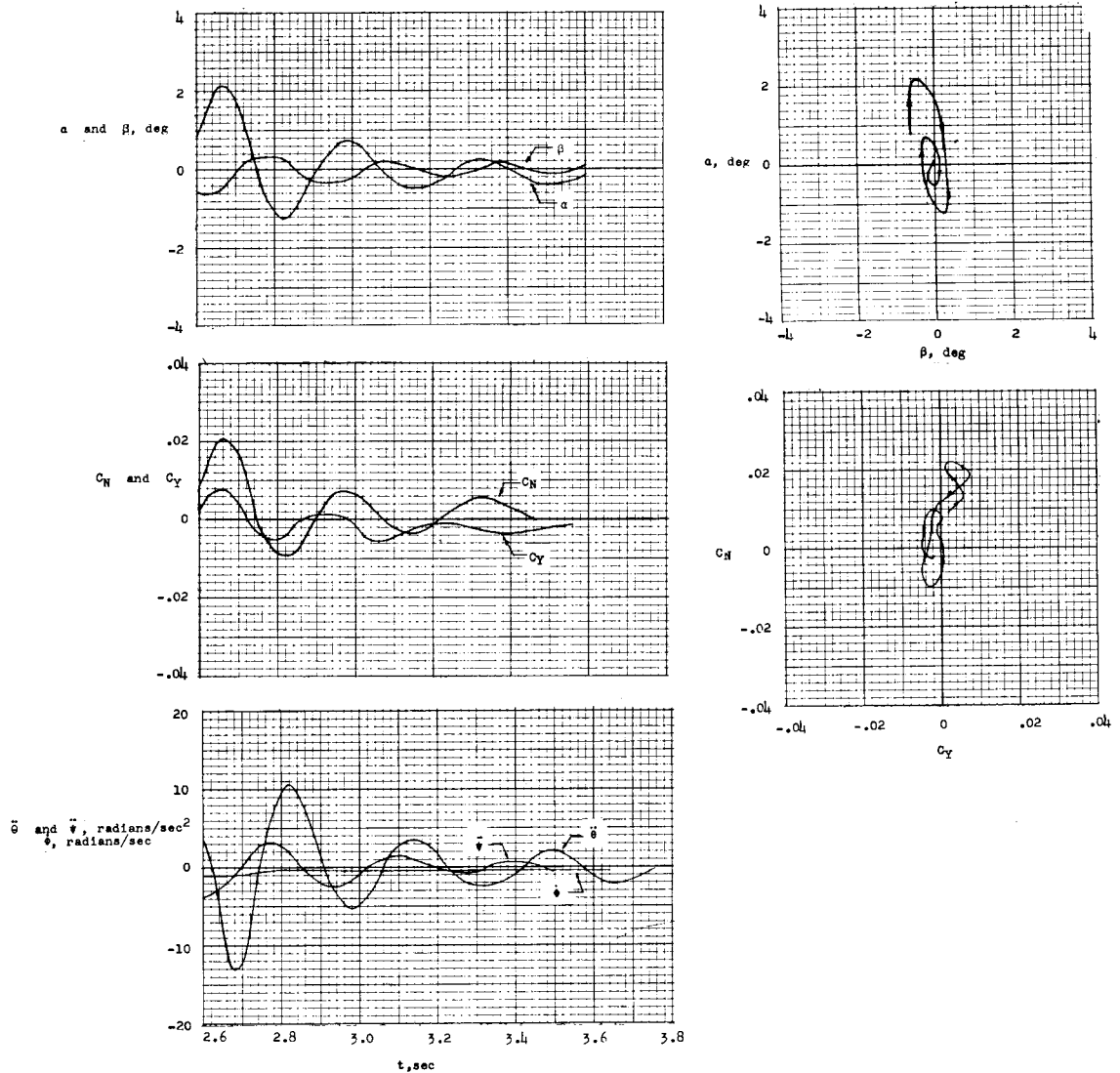
(a) Model 1.

Figure 6.- Measured angles, forces, and accelerations for short-period oscillations of the rocket test models.
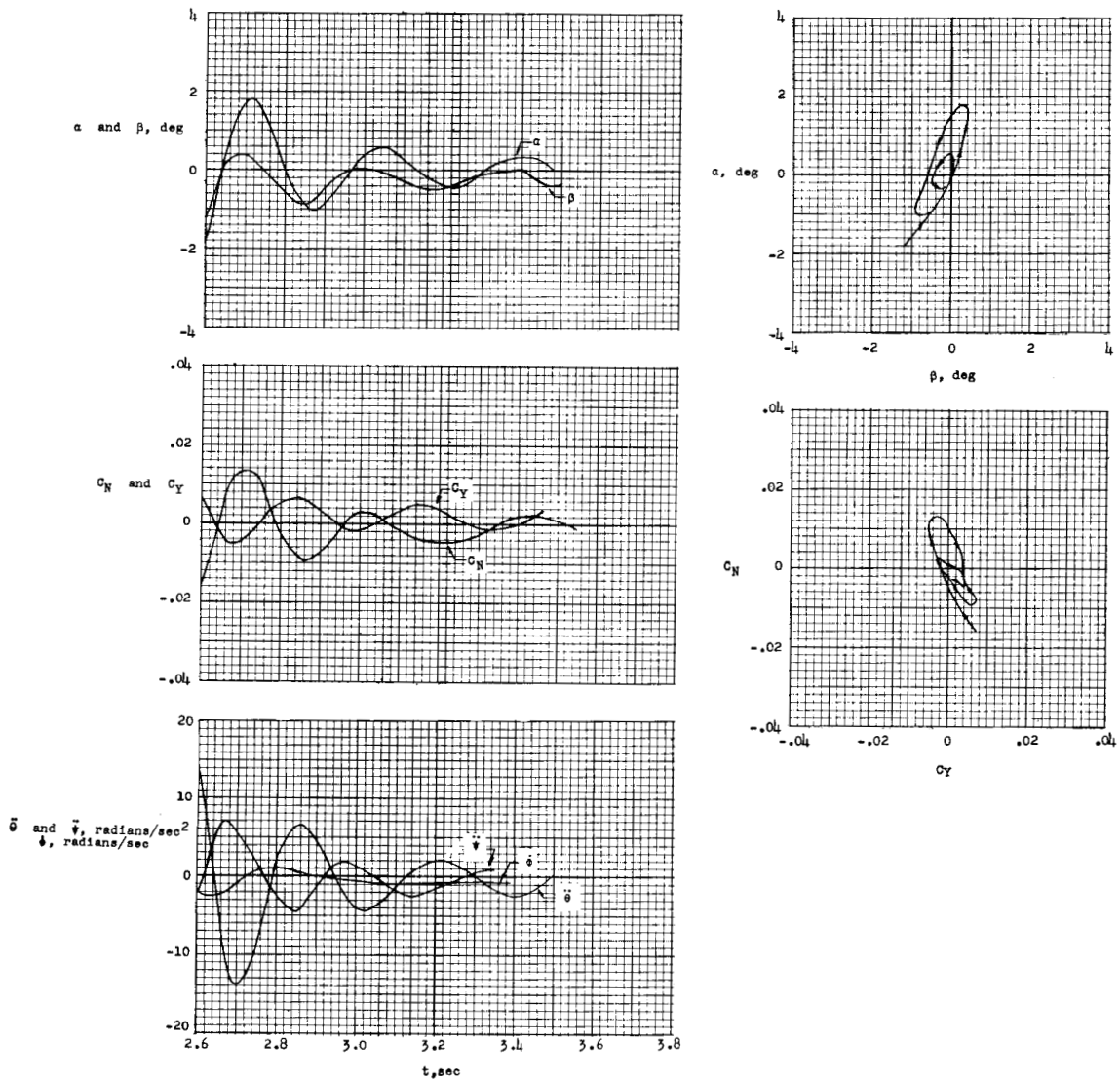
(b) Model 2.

Figure 6.- Concluded.
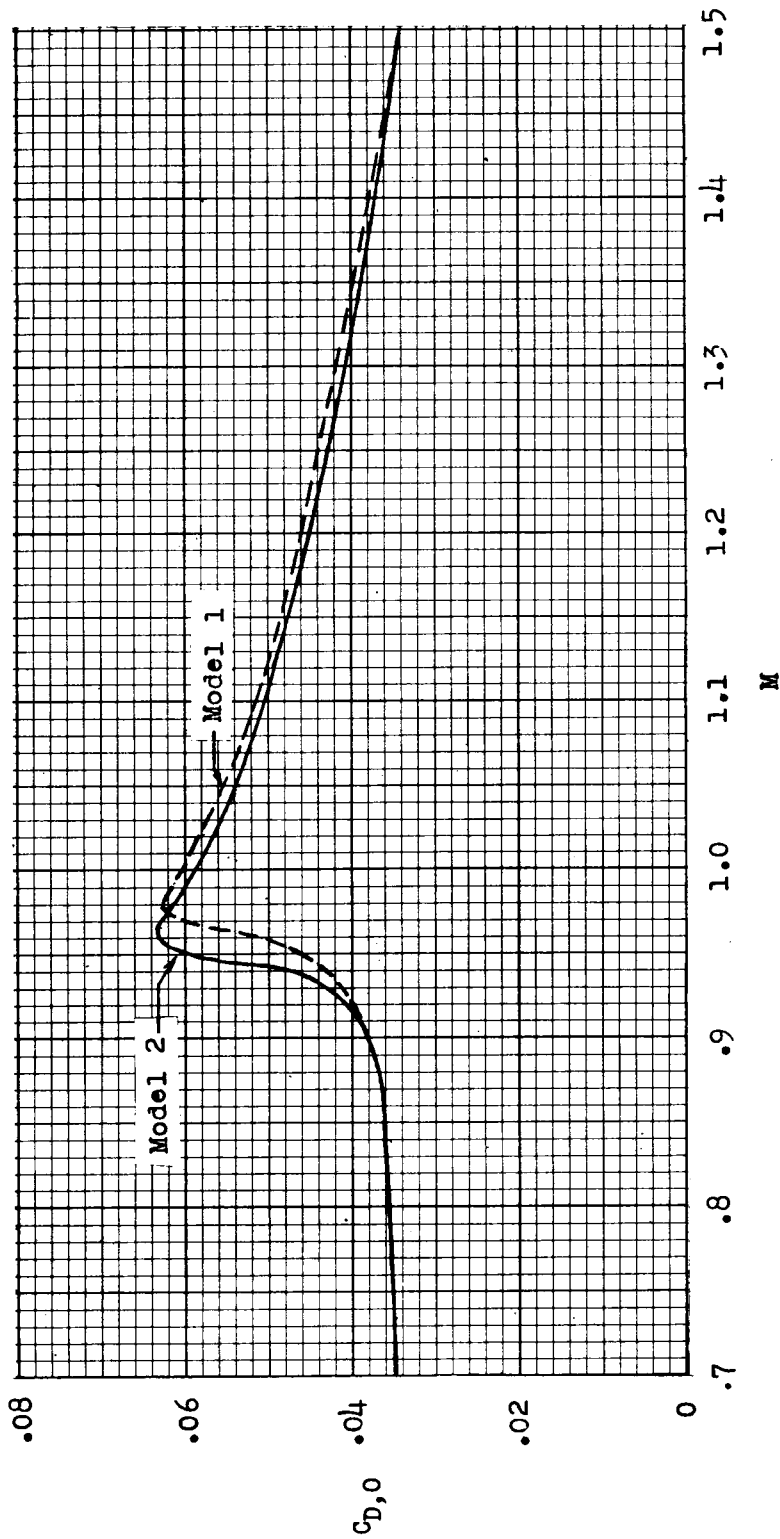
Figure 7.- Variation of total zero lift-drag coefficient with Mach number for models 1 and 2.
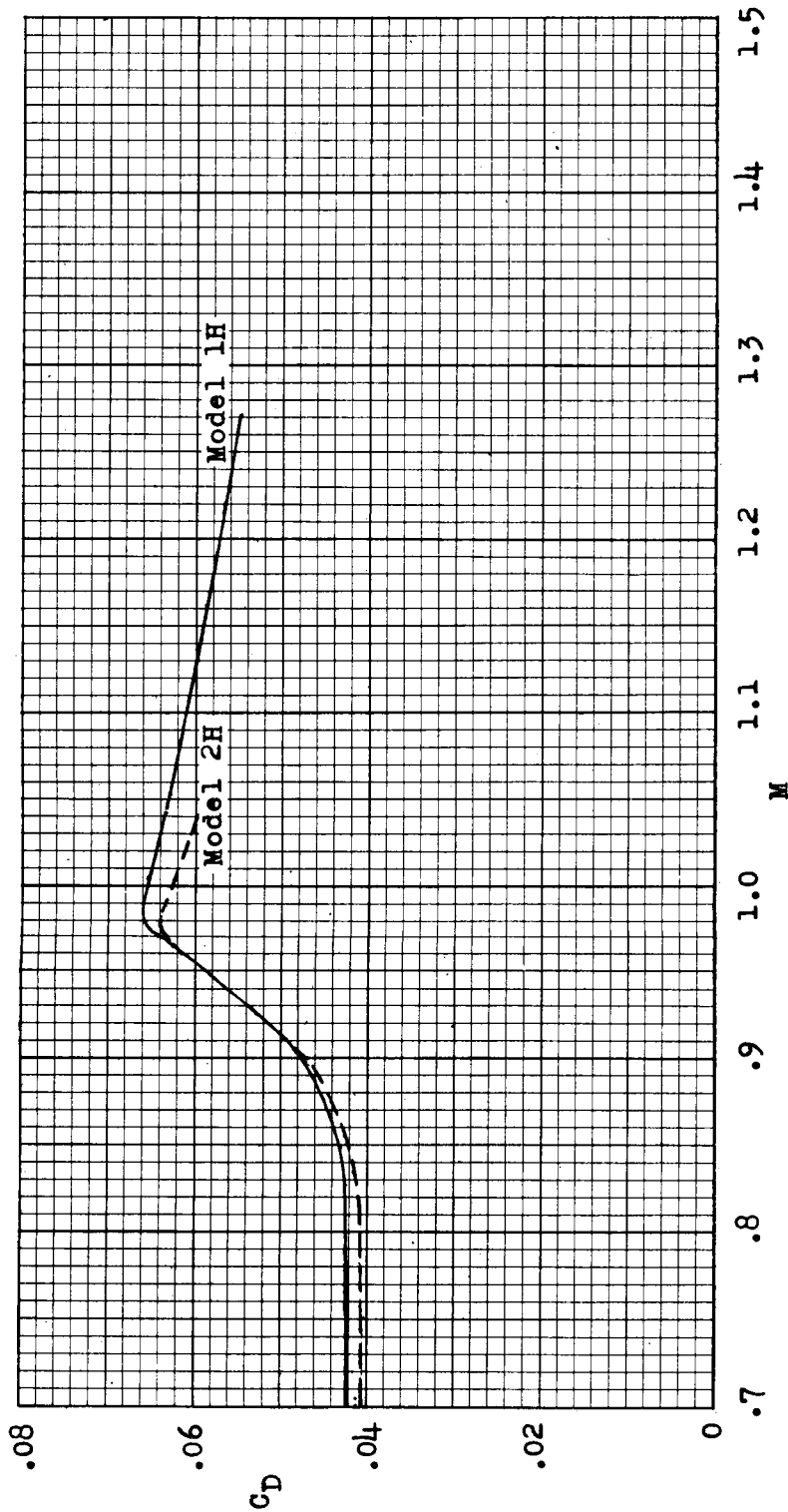
Figure 8.- The variation of total drag coefficient with Mach number for helium-gun models 1H and 2H.

24
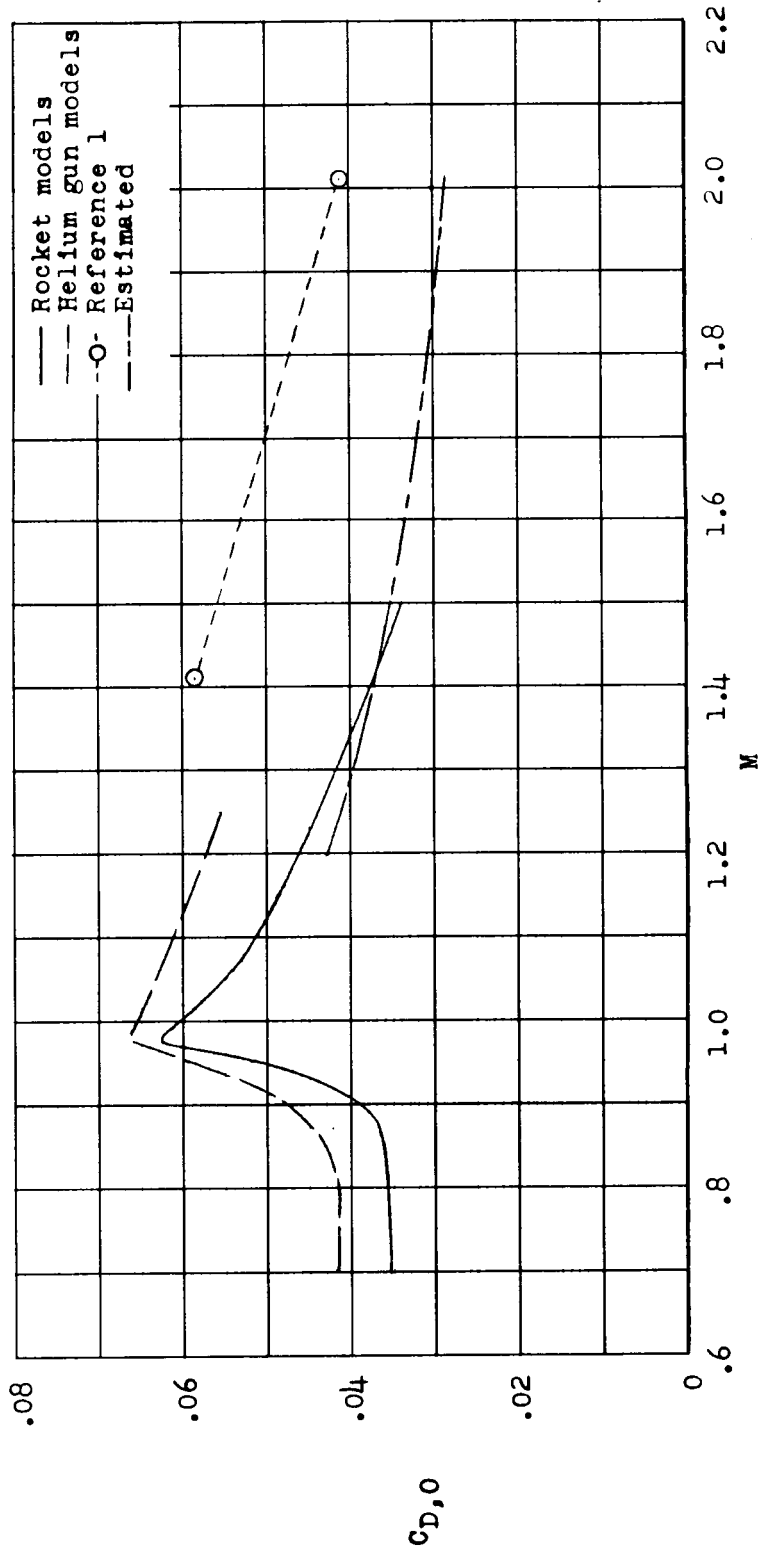
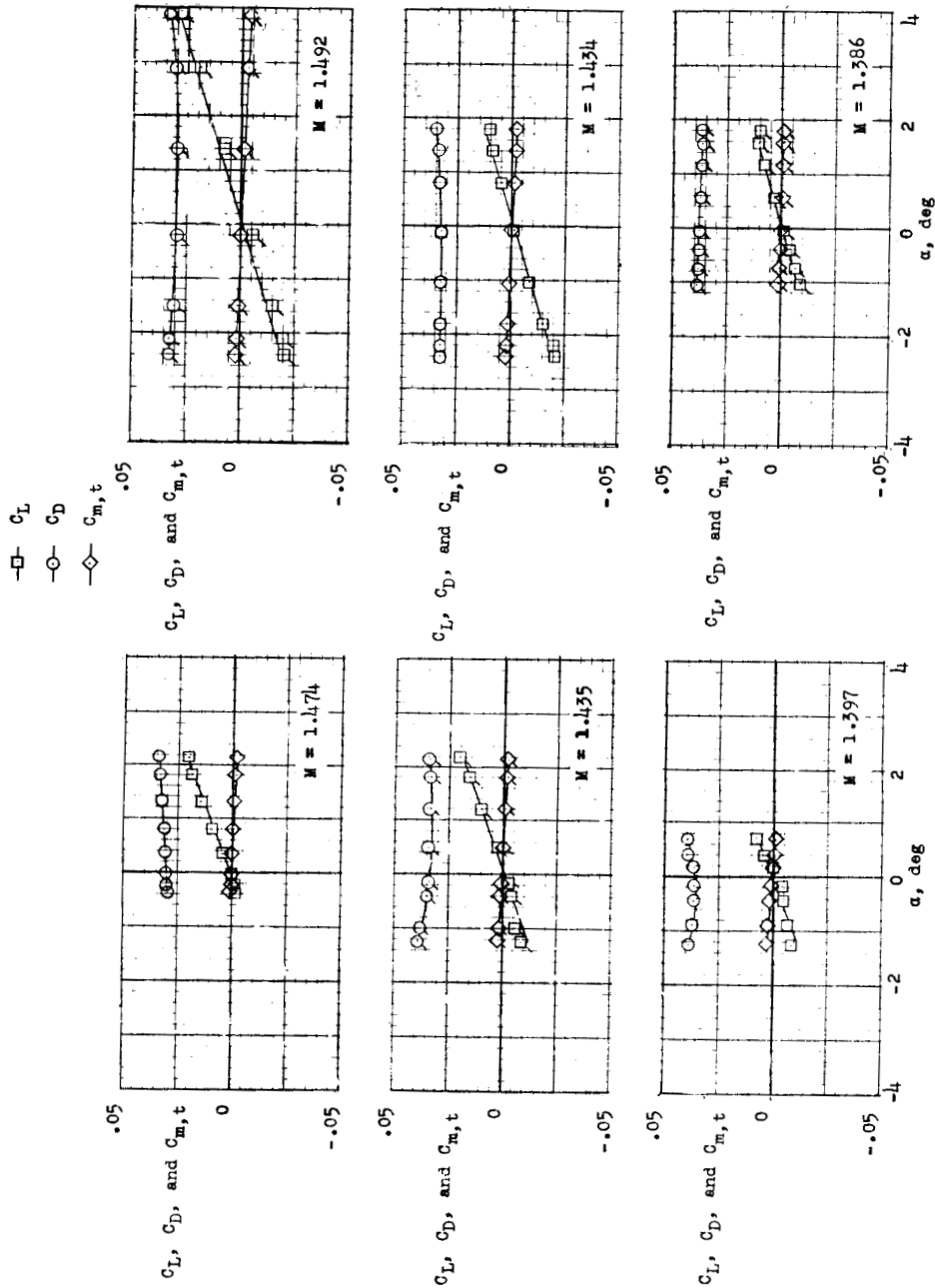Figure 9.- Comparison of measured and estimated total drag coefficients for the configurations.

(a) Model 1.

(b) Model 2.

Figure 10.- Variation of drag, lift, and total pitching-moment coefficients with angle of attack obtained during pitching oscillations. Flagged symbols indicate decreasing angle of attack; unflagged symbols indicate increasing angle of attack.
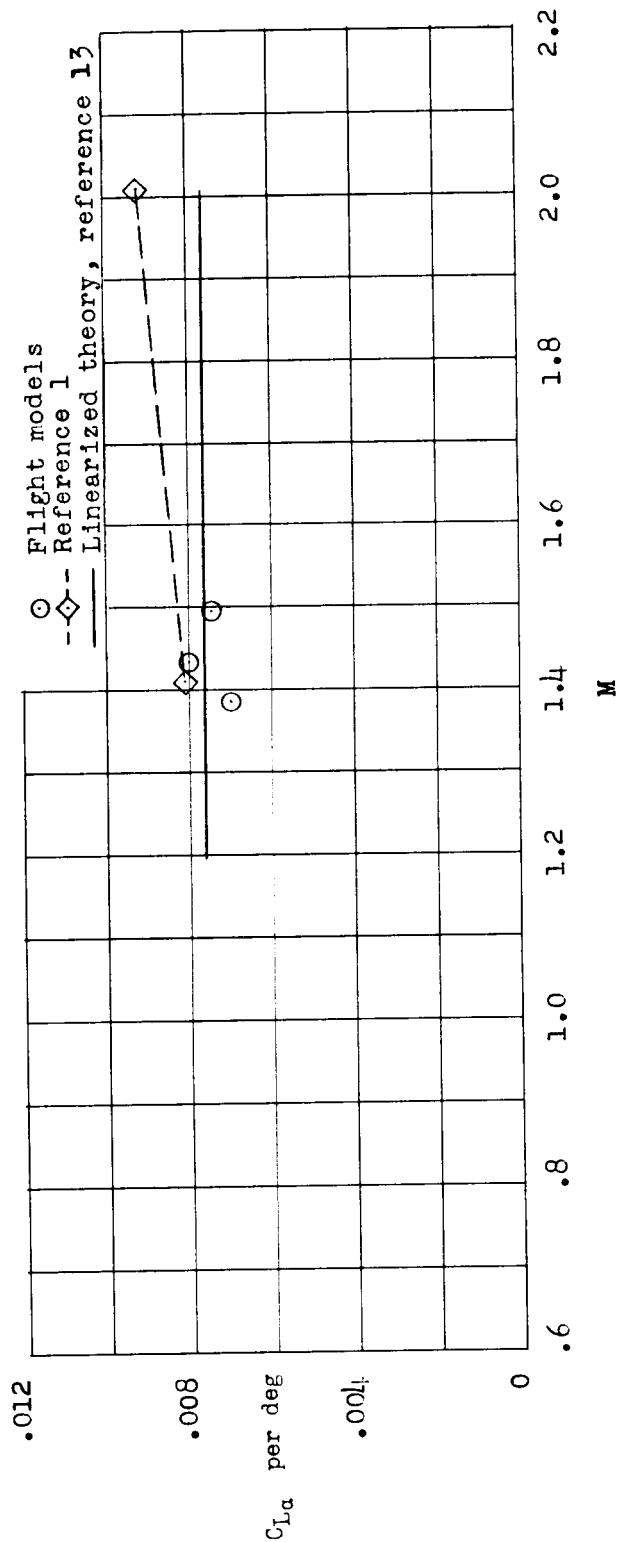
Figure 11.- Comparison of measured and estimated lift-curve slope at $\alpha = 0^\circ$ with Mach number.